Technical Paper

ISSN 1997-1400 Int. J. Pavement Res. Technol. 8(4):221-232

Non-destructive Performance Evaluation of Experimental Short Continuously Reinforced Concrete Pavement

Lucio Salles[1+], José Tadeu Balbo[2], and Deividi da Silva Pereira[3]

Abstract: As a proposed long-term pavement solution for bus stops and corridors in highly urbanized areas, four experimental continuously reinforced concrete pavement (CRCP) sections with different percentages of longitudinal steel were built in São Paulo, Brazil. The pavement sections are only 50 meters long each, a short construction length in comparison to traditional CRCP, which is normally built as long as the construction process allows. A four-year cracking survey of the experimental sections showed that the shorter section length, perhaps due in part to the lack of anchorage, results in a cracking pattern unlike that of the CRCP with traditional lengths. Additionally, two non-destructive tests were carried out to evaluate the structural performance of the experimental sections. First, deflection tests using a falling weight deflectometer (FWD) were conducted to measure the load transfer efficiency (LTE) across all cracks and to determine slab parameters by backcalculation. Second, dynamic load tests to obtain the concrete stresses under a known load. The results show that the LTE values are adequate (above 90%) in all sections, despite its distinct crack pattern and that tensile stresses at the bottom of the slab are within critical strength values for the concrete. The results from this experimental study are discussed in light of the current literature for CRCP design and performance.

DOI: 10.6135/ijprt.org.tw/2015.8(4).221

Key words*: Continuously reinforced concrete pavement; Cracking; Deflections; Load transfer efficiency; Dynamic stresses.*

Introduction

A large number of asphalt pavements at bus stops in urban corridors in tropical climates present distresses like transversal and longitudinal shoving, which are related with wheels breaking forces and high temperatures. The extent of these failures has demanded, in the past decades, the replacement of such asphalt pavements with concrete pavements. However, faulting and spalling in joints have been usual distress types in these concrete pavements for this application, inducing early-age failures. Whether problems in the design procedure or poor construction practices, flaws in the contraction joints and in their dowels bars are key indicators of unusually weak performance in JPCP [1]. Joint-related distresses are highly influential to the pavement's ride quality, as shown by Liu et al. [2], therefore, if most failures of JPCP in this application are joint-related, why not use a concrete pavement without joints?

Several studies point out that the major qualities of the continuously reinforced concrete pavement (CRCP), a concrete pavement without contraction joints, are its durability and low maintenance needs, making it a very suitable solution for bus corridors in Brazil [3-7]. With these assumptions, it was decided to build the first CRCP in Brazil in order to analyze the pavement performance in a tropical environment. Some previous studies with traditional CRCP suggest caution is taken in the construction of CRCP in high temperatures [8, 9]. In response to these concerns, experimental short-length sections were proposed for bus stops in urban corridors that are usually asphalt pavements or JPCP. These sections were monitored and tested to determine their suitability as a replacement to asphalt or JPCP. This paper presents the results of that study, which includes:

- Crack pattern analysis, discussing its differences from traditional CRCP one;
- FWD loadings for two non-destructive tests performed to evaluate the CRCP structure;
- Truck axle load over instrumented section to evaluate the CRCP response.

Short-length CRCP Test Sections

The four short CRCP sections (constructed September 2010) are located near a bus terminal in front of the civil engineering building at the campus of University of Sao Paulo. The daily traffic is composed of over 800 urban buses per day along with some dozens of medium trucks and 1,500 cars. The sections are 50 m long and 5.05 m wide. The pavement layers are composed equally in all sections by a dry macadam sub-base (300 mm), a hot asphalt mixture base (60 mm) – reports from other studies show that asphalt bases work better than granular or cemented ones [6, 10] – and a concrete slab (240 mm); the only difference between sections is the longitudinal reinforcement steel percentage: Section 1 (0,6%); Section 2 (0,7%); Section 3 (0,4%) ; and Section 4 (0,5%). The longitudinal reinforcement is placed 20 mm above the slab half-height. Between sections 1 and 3 and sections 2 and 4 are dowels bars as they are constructive joints. Transversal bars are always spaced of 0.9 m in any section; all bars diameters are 20 mm (steel ultimate strength of 500 MPa). Concrete design flexural strength was 4.5 MPa (28 days). Further details on construction

[1] Av. Prof. Luciano Gualberto, 380, Cidade Universitária, São Paulo, CEP 05508-010, Brazil.
[2] Department of Transportation Engineering, University of São Paulo, Brazil.
[3] Department of Transportation Engineering, Federal University of Santa Maria, Brazil
[+] Corresponding Author: E-mail lucio.salles@usp.br
Note: Submitted August 13, 2014; Revised April 19, 2015; Accepted April 21, 2015.

practices can be found elsewhere [11].

Short CRCP Crack Pattern

CRCP long-term performance depends on its early age performance, as emphasized by Zhang & Wang [12]. In accordance to this, the first crack surveys were carried out in weeks following construction. No cracking was observed in any sections. Successive surveys were carried out monthly with similar results. It was only in October 2011, one year and two months from the opening of the sections to traffic, that the first cracking was observed in the sections (Section 3). From this first crack, five more cracks were found in Section 3, and three in Section 4 in January 2012. Fig. 1 shows the result of all surveys and allows the cracking analysis with time. The horizontal arrows point out the traffic direction in each lane.

The major difference between the evolution of cracking in short-length CRCP sections and the traditional CRCP is the time until cracks appear at the pavement surface after construction. As shown by several examples [3, 6, 13, 14], traditional CRCP is expected to have cracking within two months after construction, if not immediately after. Also, the full crack development should last no longer than two years [3]. It took more than one year for the first crack to be visible on the concrete surface; and even after two years, Section 2 has only two cracks and Section 1 has yet to present any crack. Considering that the experimental short CRCP has conventional layers and materials as CRCPs found out in former publications, it is only reasonable to believe that the unlike crack development is due to its short length along with the unbounded concrete/asphalt base interface. Common concrete knowledge says that a 50-meter long concrete surface with no cracks is very unlikely to happen; one should consider that cracks are present within all the slabs from the construction time and concrete curing. However, those cracks are not evident due to three fundamental reasons, namely: firstly, the short length; secondly, no anchor system exists at the end edge of any slab, what *per se* allows horizontal displacement of the slab volume; thirdly, the concrete was laid over a hot mix asphalt base course, creating a strong bond breaker interface between slabs and bases when compared to cement bound bases or rolled compacted concrete, therefore making it easier again for the fresh concrete mass to slip over the base during concrete initial contraction. This very particular combination of short length and slipping freedom helps to conceal the shrinkage mechanism but not to avoid it; the cracks are still there, only refrained from appearing in early times, due to the strong tying effects of the longitudinal bars.

In contrast to traditional CRCP, the steel percentage had an inverse influence on the cracking process. It was expected that sections with higher steel ratios would present more cracks, however, sections 3 and 4 show less cracks than Section 1 and 2 [6, 15]. Evidences on why this is happening can be found when analysing the air temperature data during August 2010 (construction month) in Fig. 2. Firstly, all sections were built in cool morning temperatures (between 10 ℃ and 16 ℃). The major difference was the temperature variations in the days that followed; for Section 1 there was a huge drop of more than 20 ℃ on the next day, however, in the following days, the day and night temperature changes was milder than for the remaining sections. Section 3 and 4 faced more harsh fluctuations; day and night temperatures changes impact the

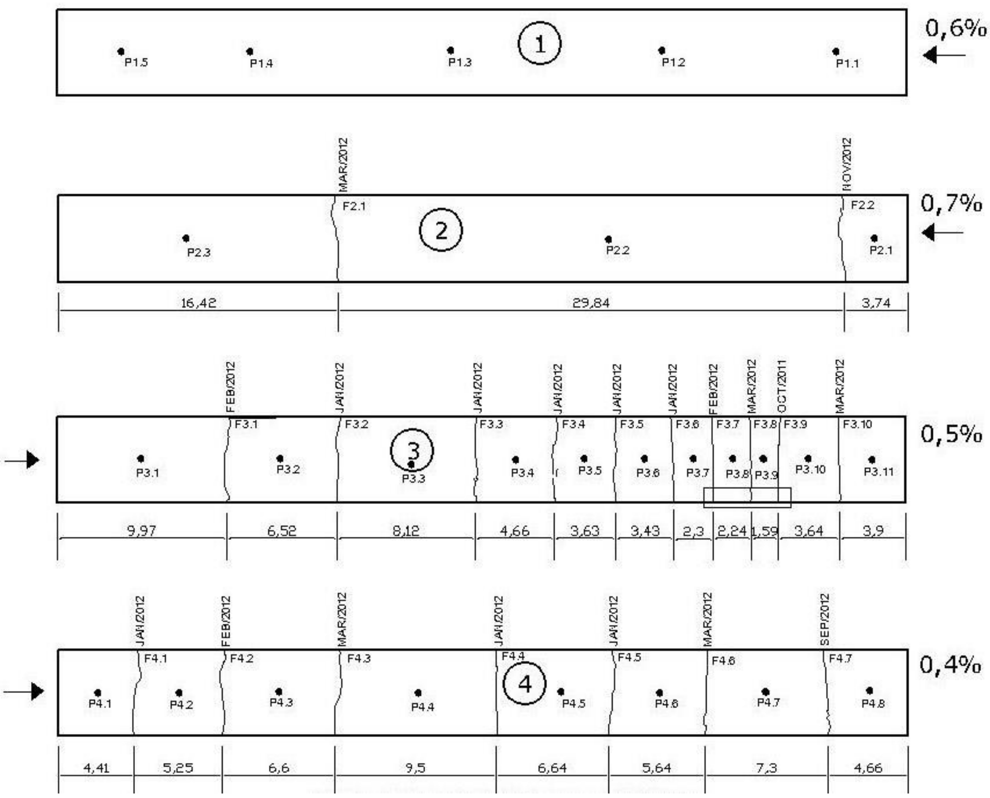

Fig. 1. Short-length CRCP Sections Cracking.

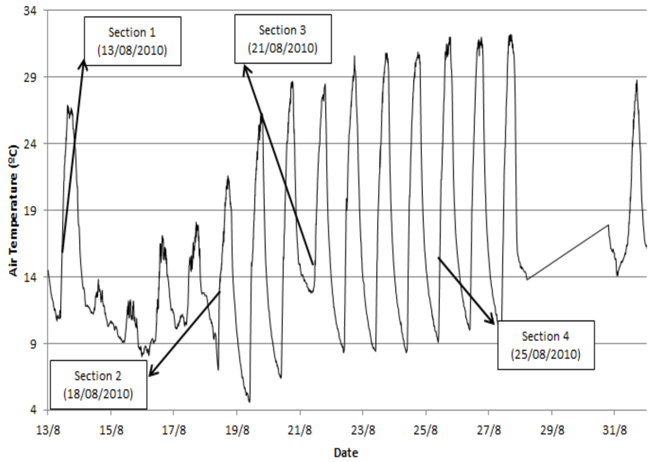

Fig. 2. Air Temperature During the Construction Month.

slab thermal gradient, which, is related to the slab warping. As the curing process was the same for all sections (burlap and water spraying), Section 3 and 4 suffered from more severe warping during the following days. This can explain the development of more cracks at the slab's surface on those sections.

Concerning the crack's shape, Section 3 and 2 show divided cracks, two in Section 3 and one in Section 2; as known this kind of crack is non-desirable because its intersection can potentially evolve into future punchouts [3]; regarding the meandering shape, all cracks are pretty tight and uniform, showing no potential for future intersections. Some minor spalling was found in two cracks in Section 3, whether this problem will evolve or not remains to be seen. Spalling affects the traveling public impression on the pavement ride quality and in a long-term period can reduce the LTE values across cracks [16].

Crack Spacing and Crack Width

Fig. 3 shows the average crack spacing through time and the crack spacing percentage distribution in sections 3 and 4; in Fig. 3(a) the section length was considered as the initial crack spacing; this value only changed with the first crack appearing on October 2011 in Section 3, almost 400 days after construction. Once the first crack showed up, the crack spacing decreased more rapidly in sections 3 and 4 reaching a standard in two years. In Section 2 the first visible crack only appeared 500 days after construction and differently from Sections 3 and 4 the decrease in the average crack spacing has being slower. The short CRCP average crack spacing (Sections 3 and 4) is more than double of that found in traditional CRCP; a difference aggravated by the fact that for the latter the crack spacing standard is reached in less than a year. The vertical lines in Fig. 3(b) mark the crack spacing interval recommended by the AASTHO Design Guide [17]; the graph shows that only 27% of the Section 3's crack spacing is regarded as ideal; also for both sections there is no crack spacing less than 1.5 m, implying a very small possibility of cluster cracking and punchout development. Regarding punchouts, no examples of the distress in crack spacing bigger than 1.5 m was found formerly on literature. Experience with traditional CRCP shows that the cumulative crack distribution reaches 100% with crack spacing bellow 3.0 m for a two-year old pavement and

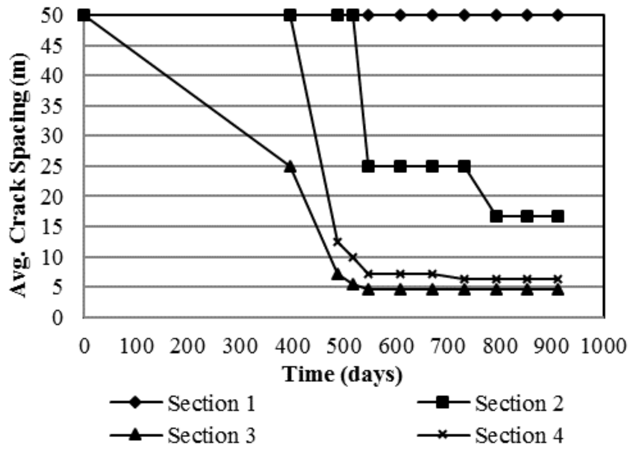

(a)

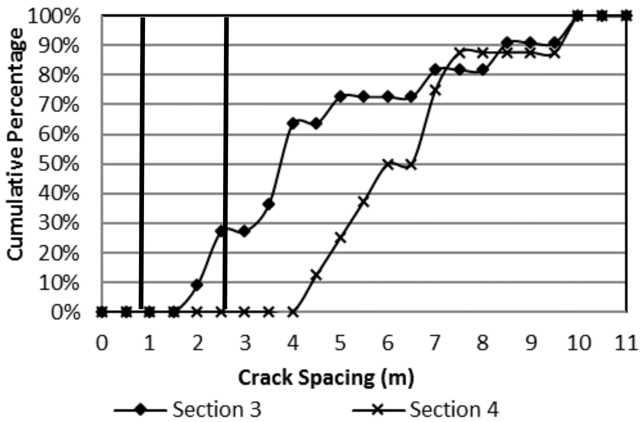

(b)

Fig. 3. Crack Spacing: (a) Average Through Time; (b) Percentage Distribution.

the AASTHO recommendation range comprehends between 50 and 90% of crack spacing for a CRCP with good performance [8, 13, 14].

Crack surveys confirmed the influence of steel percentage and mostly temperature in crack width. The crack width measurement was performed with a millimetre graduated ruler; this method, although fast, allows only the surface measurement. Average crack width, in the last survey dated August, 2013, for Section 2 was 0.17 mm; Sections 3 and 4 average crack widths were 0.55 and 0.33 mm, respectively; the average temperature during the survey was 16℃. In contrast, on a hot January, 2014 day, the average crack widths were 0.1 mm (Section 2); 0.37 mm (Section 3); and 0.26 mm (Section 4). The temperature reached 27 ℃ on that particular day; the two cracks in Section 2 were barely visible. A more precise method for crack width measurement that can provide the crack width in any slab depth is being developed. Despite the method, the crack width values were similar to others found elsewhere [13, 14].

Non-visible Cracks Hypothesis

As discussed, the idea of a 50-meter length concrete surface without joints and cracks seems very unlikely to happen. The hypothesis that the cracks were in the slab but not visible due to a non-anchoring structure and slipping freedom was tested using FWD testing and analysis conducted in December 2011.

The FWD plate was always located at the intermediate portion of one section (25 m from either transverse edge) and one meter from the longitudinal edge. Fig. 4 shows the real-field deflection and the theoretical-backcalculated deflection basins (using EVERFEE software [18]) for each section. It is remarkable in Fig. 4 that there were some difficulties to match field and backcalculated deflection basins for Sections 3 and 4 at their 900 mm offsets, while for Sections 1 and 2 the backcalculation process was easy like six successive interactions. The reason for the discrepancies found in Sections 3 and 4 may be tied to the existence of cracks yet not apparent to naked eye during the survey in October 2011. Fig. 1 illustrates that those invisible cracks, if were in fact present, appeared later in the next survey. In the January 2012 survey, Section 3 showed a visible crack 25.39 m far from the slab end; the same happened to Section 4, with a crack located 24.24 m from the transverse joint. Section 2 did not present basin matching problems, thus it should not be expected that a crack would develop around the middle of the slab in the upcoming months; Fig. 1 supports this assumption as well. Nevertheless, other factors could contribute to variation in response under FWD testing and cannot be ruled out at this point.

Falling Weight Deflectometer (FWD) Testing

In order to assess the LTE across cracks, the simplest and most routinely method is the one introduced by [19]. In this method the FWD plate position, related to the crack's location, must be such that allows symmetrical deflection measurement, i.e., at least two sensors must be equally distanced from the crack, one at the loaded slab and the other at the unloaded slab. The calculation is performed trough Eq. (1), as follows.

$$LTE = \frac{\delta_2}{\delta_1} \times 100[\%] \tag{1}$$

where δ_1 is the deflection of the loaded slab and δ_2 is the deflection of the unloaded slab.

Based on a study with JPCP [19], it was suggested a minimum LTE of 75% as an adequate structural performance indication; another former study [20] showed, again for JPCP joints, that in new pavements without dowel bars, the LTE was between 70 and 100%, and that for new dowelled pavements the lower limit was 80%; the study author considers unacceptable a LTE lower than 70%.

In the present study, the load was fixed at 60 kN as to obtain a more detailed assessment of deflections given the high stiffness of a concrete pavement with high steel reinforcement ratio. Also, the FWD was applied between cracks to allow the backcalculation of the elasticity modulus of concrete (E) and the subgrade reaction modulus (k). As Section 1 exhibited no cracking, it was used exclusively for the parameterization study. All load application points are shown in Fig. 1 (where F stands for crack position and P for applications between cracks).

Deflection Basins

The deflections obtained at the crack (F points) and between cracks (P points) enabled the deflection basins layout as seen in Figs. 5 and 6. By analyzing the graphs, it is easily noticed that the site with the biggest deflection is near Section 1's edge; at this region, near the joint, there is a interlocked pavement presenting deformation; a vertical bump is felt whenever a vehicle access the CRCP. Nevertheless, the higher deflection values are always located near the joint in a direct relation to the slab lack of anchorage allowing slab free movement, therefore increasing the deformations. The lowest maximum deflection values are those located near the slab's center, as expected. In an experimental JPCP placed near the experimental CRCP sections, it was observed that joints without dowel bars experienced much higher displacements than those presented by joints with dowel bars [21]. Although the joints

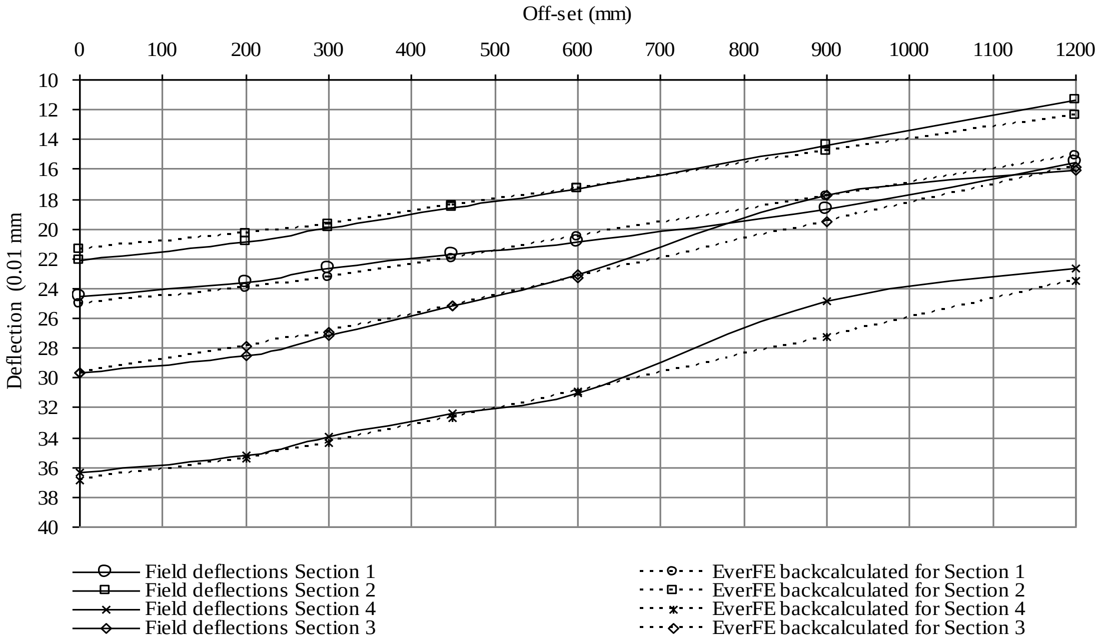

Fig. 4. Field and Theoretical Deflection Basins.

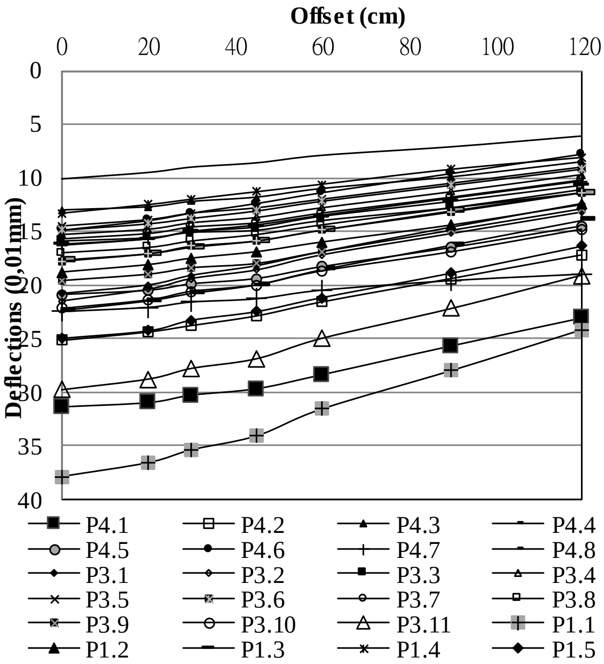

Fig. 5. Deflection Basins at between Cracks Position.

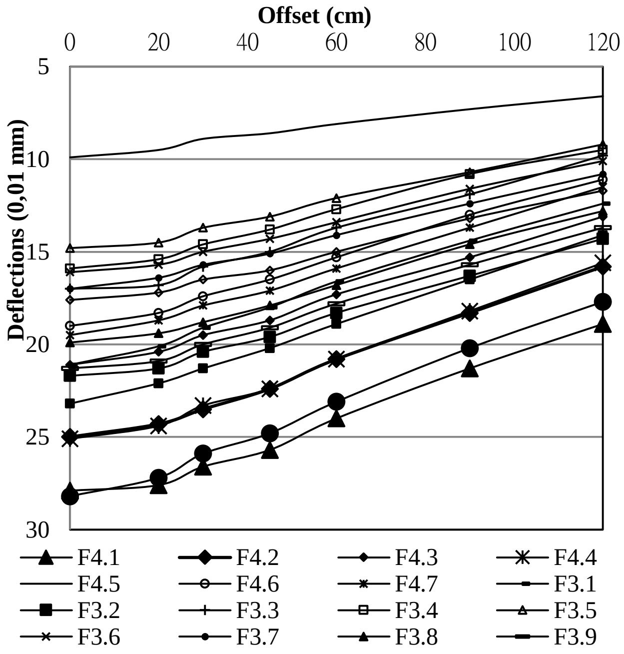

Fig. 6. Deflection Basins at Crack Position.

(cracks) in CRCP do not have dowel bars, the small crack width in addition to the tightening strength provided by the longitudinal steel hold the slabs together increasing stiffness and reducing the deflections even in a physical discontinuity. Also, the comparison between deflections at the crack and between cracks reinforces these assumptions. As for the shape, basins appear a typical rigid pavements outline with a smooth decrease of deflections through the sensors.

Load Transfer Efficiency (LTE) Across Cracks

The FWD test applied tangential to the crack provided equidistant deflection data between the loaded and the unloaded slabs. Fig. 7 shows the LTE values for each crack and disclose the following findings:

- All cracks presented a LTE value greater than 90% (92.7% average);
- It was not possible to observe any influence of the longitudinal reinforcement percentage in LTE; it was expected that the Section 2 cracks would show a higher LTE, however the three sections average LTE was very similar;
- Section 2 with the lowest average crack width was expected to exhibit a higher LTE. However, the crack width measurement was only able to determine the crack width at the surface; little is known about the crack width through the slab's depth;
- The crack with the lowest LTE (90.52%) is F3.1, positioned at Section 3 end (Fig. 1); yet strangely, the crack with the highest value of LTE (95.51%) also lies in a section limit (Section 4). Deflections were quite high in this position as seen in Fig. 5, however, more or less displacement does not seem to influence the crack load transfer performance;
- As some researchers state, the influence of crack spacing in

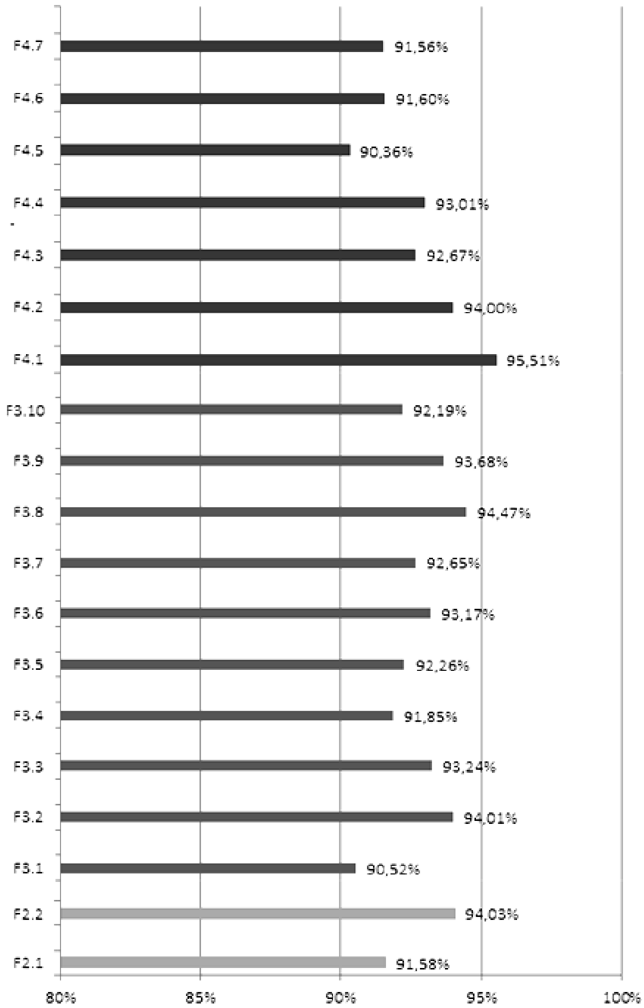

Fig. 7. LTE for Cracks.

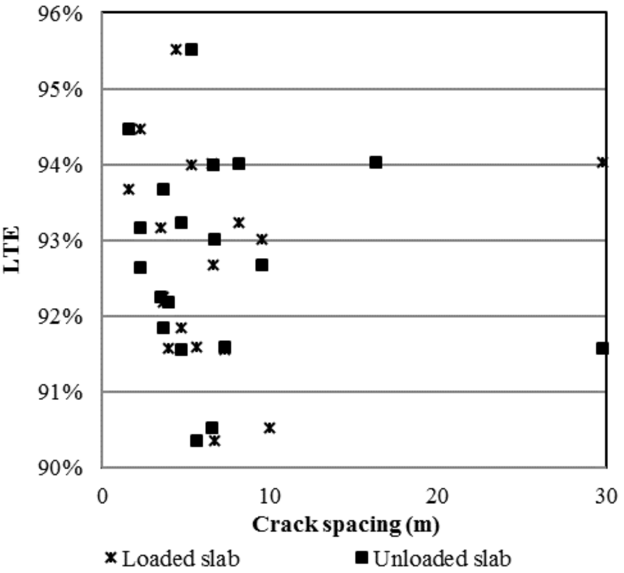

Fig. 8. Crack Spacing Versus LTE.

LTE was not observed [7, 15]. Fig. 8 shows the relation between the LTE and the crack spacing in the loaded and unloaded slab. Note that no trend is visible, *i.e.*, very large crack spacing, as those showed by Section 2, are not harmful to the load transfer. This relation could change with time if crack deterioration becomes evident.

- When simulating a crack in the FWD applications between cracks (P points), the fictitious LTE is quite similar to the real LTE, thus, strengthening the CRCP structural integrity. The results for the fictitious LTE can be found on Table 1.

Parameterization

The backcalculation process, through real and theoretical basin matching, enables the determination of the E and k parameters. The theoretical deflections were obtained using the EverFE 2.24 software; although the software was designed for JPCP analysis, it is possible to simulate other structures, given a known geometry. Thus, in the CRCP case, the cracks were considered as joints without dowel bars. It should be noticed that the longitudinal steel in CRCP does not carry load like a dowel bar, its major role is to keep the cracks tightly closed [22]. So, the load transfer between cracks happens exclusively by aggregate interlock, which is related to the joint/crack stiffness. The input values of crack stiffness applied to the software were based on a correlation between crack width and crack stiffness [23]. The preliminary input values of E and k were estimated according to the studies found elsewhere [24, 25]. The basin matching process was conducted with as many simulation trials necessary to reach a minimum square error, which was calculated by Eq. (2), as follows.

$$Square \quad Error = \sum (d_i^{real} - d_i^{theoretical}) \tag{2}$$

All FWD tests between cracks and in Section 1 (P points) were considered for backcalculation. Table 2 brings the E and k along with the square error found in all P points. During the process, it was observed that the matching theoretical deflections near the edge were very high, thus providing low E and k values. This can be explained by the lack of anchorage, that allows free vertical movement of the slab edge, and consequently causes higher deflections; and, because of those higher displacements, the concrete suffers from heavy vehicles impact resulting in early concrete deterioration. As expected the site P1.1 presented the lower E and k due to the higher deflections caused by the joint-failure defect between the CRCP and the interlock pavement. Section 2 presented the bigger E and k; in fact even when the loading point was near the edge the values remain higher than some middle slab points in other sections; this can be explained by a larger percentage of steel reinforcement in Section 2, which increases the pavement stiffness.

Dynamic Load Testing

The slab chosen for analysis was that of Section 3 because it exhibited more cracking and thus a smaller crack spacing. The

Table 1. Fictitious LTE between Cracks.

Ponto	Deflections (0.01mm)		LTE	Ponto	Deflections (0.01mm)		LTE
	0	300			0	300	
P4.1	31.4	30.3	96.50%	P3.7	15.7	14.6	92.99%
P4.2	25.2	23.8	94.44%	P3.8	17.0	15.9	93.53%
P4.3	13.0	12.2	93.85%	P3.9	19.6	18.4	93.88%
P4.4	22.4	20.8	92.86%	P3.10	22.2	20.6	92.79%
P4.5	20.9	19.9	95.22%	P3.11	29.8	27.8	93.29%
P4.6	14.9	13.3	89.26%	P1.1	37.9	35.4	93.40%
P4.7	16.3	15.0	92.02%	P1.2	18.8	17.5	93.09%
P4.8	17.7	16.5	93.22%	P1.3	16.2	15.0	92.59%
P3.1	20.8	19.1	91.83%	P1.4	13.3	12.0	90.23%
P3.2	21.5	19.4	90.23%	P1.5	25.0	23.3	93.20%
P3.3	15.9	15.1	94.97%	P2.1	22.5	21.6	96.00%
P3.4	15.3	14.2	92.81%	P2.2	10.1	9.0	89.11%
P3.5	14.5	13.3	91.72%	P2.3	17.8	16.4	92.13%
P3.6	14.9	13.8	92.62%				

Table 2. Backcalculated E and k for each FWD Point

	Section 1					Section 4							
Ponto	P1.1	P1.2	P1.3	P1.4	P1.5	P4.1	P4.2	P4.3	P4.4	P4.5	P4.6	P4.7	P4.8
E (MPa)	12,000	35,000	34,000	38,000	28,000	25,000	27,000	45,000	25,000	30,000	28,000	32,000	30,000
k (MPa/m)	53	95	120	160	70	53	70	145	85	85	155	125	115
Erro^2	17.18	0.53	0.43	0.39	1.12	0.96	0.29	0.22	0.21	0.56	0.24	0.29	0.27

	Section 2			Section 3										
Ponto	P2.1	P2.2	P2.4	P3.1	P3.2	P3.3	P3.4	P3.5	P3.6	P3.7	P3.8	P3.9	P3.10	P3.11
E (MPa)	30,000	60,000	35,000	25,000	25,000	30000	35,000	42,000	38000	42,000	42,000	28,000	28,000	25,000
k (MPa/m)	80	200	105	95	95	120	130	135	135	115	105	100	85	60
Erro^2	17.23	0.16	0.11	0.37	0.90	3.60	0.22	0.23	0.20	0.44	0.27	0.44	0.48	0.82

rectangle in Fig. 1 highlights the instrumented area position in Section 3 layout. On a dry day in February 2013 (with air temperatures of approximately 20℃), the gutter removal and excavation was carried out. A styrofoam partition had been place at construction to separate the slab from the concrete gutter, which made the slab side fairly regular and smooth, therefore facilitating the placement of instruments above the slab middle side. The existence of a "concrete foot" formed during construction, in the last few inches of the slab, due to the 20 cm depth of the gutter, was also noticed. After the complete removal of the gutter, the surface and lateral side of the slab were polished with an electric grinder followed by a slab sweep to remove concrete dust. After that, the strain gauges (SG) were glued to the concrete slab. Fig. 9 illustrates the position of each SG in the test segment.

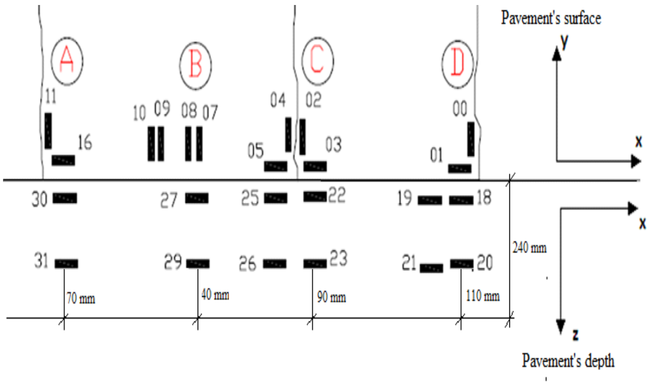

Fig. 9. Final SG Layout.

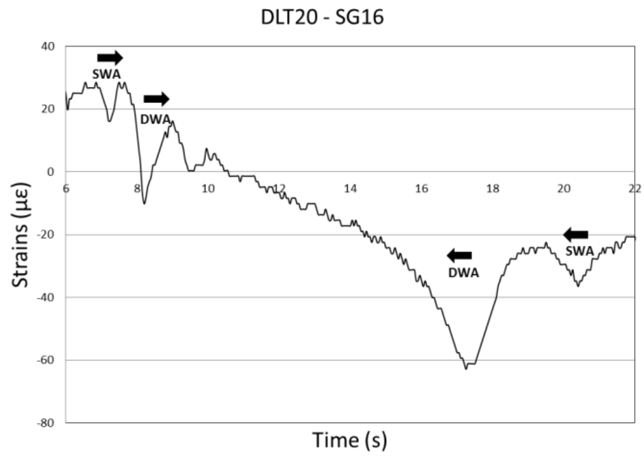

Fig. 10. Axles Operation in DLT20.

Dynamic Load Testing: Process

The truck used in the experiment was a tipper body vehicle with a single wheel axle (SWA) in the front and a rear dual wheel axle (DWA), which weighted, respectively, 3,910 and 12,580 kg. As the main goal of the dynamic load testing (DLT) is to create a database of responses and verify, by comparing real and theoretical stresses, the calibration of a stress analysis software, surveys should be conducted in order to document precisely the vehicle axis position to that of the SGs. For this, digital cameras recording the axle load testing were used. To determine the distance between axles and SGs, a strip of exactly 30 cm was marked with ink on the slab edge. The tests comprehend twenty DLTs, being fifteen with constant speed of 10 km/h, two with braking in the segment middle and three with higher speed (40 km/h). The data were acquired with a frequency of 20 Hz by means of signal amplifier connected to the SGs.

Firstly, to visualize and understand the signals of the two axles passing through the instrumented segment, in Fig. 10, the deflection versus time graph is shown. In it are explicit strains caused by truck axles during dynamic load test 20 (DLT20) at SG 16; the DLT20 was performed with an average speed of 10 km/h and braking in the position of SGs 08 and 07. SG 16 was chosen because this instrument collected the resulting deformations from the two axles. As the truck stopped in the SGs 08 and 07position, the only SG capable of measuring both strains in braking load tests were SGs 11, 16, 30 and 31.

To check the load effect in a deformation versus time graph is necessary to visualize the deformation changes; one should be careful in analyzing the data since external factors can often change the instrument deformation reading. In the case of SG 16 the vehicle axle's passage is clearly noticeable in the following sequence: at 7.2 seconds, the SWA arrived at the exact SG 16 location causing the first decreasing strain peak, a second later came the DWA, which caused the second peak, the truck stopped in the segment center at 9.2 s where it remained for approximately 8 s; at 17.2 s, accelerating in reverse, the DWA again passes by SG 16 creating the third peak and is followed by the SWA 3 s after, finalizing the complete operation with the fourth peak. As SG 16 was positioned on the slab surface, it was expected that the stresses generated by the load were compressive stresses, which was confirmed by the test.

The tensile stresses (σ) generated in a specific direction of the SG are the product of the differential deflection between the maximum states of tension and relaxation (Δε) and the material elasticity modulus. Fig. 11 illustrates the calculation method. The elasticity

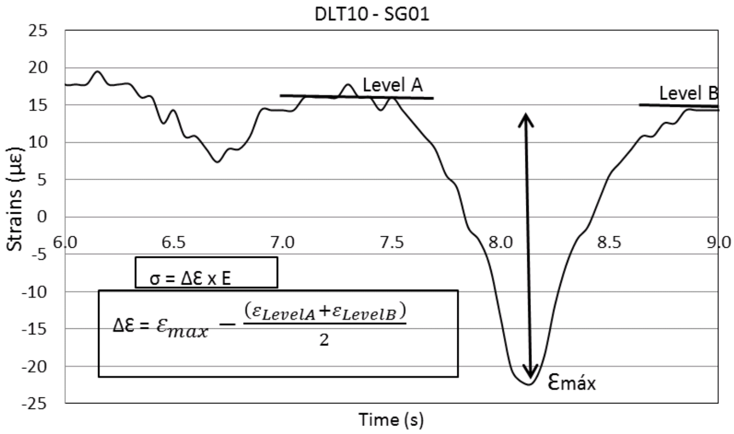

Fig. 11. Stress Calculation Method in DLT10.

modulus of concrete was that backcalculated for the parameterization section. As the DLTs were held at the points P3.8 and P3.9, the values for these slabs displaced in Table 2 were used. Tables 3 and 4 bring all the stresses measured at the test.

Stress analysis

As anticipated, the stresses generated by the SWA were lower than those of the DWA. Also as expected, the surface and top longitudinal SGs measured negative strain peaks, thus producing compressive stresses; on the other hand, the bottom SGs captured positive strain peaks, generating tensile stresses. At the surface, the transversal SGs measured positive strains. Those orthogonal SGs at the surface were able to measure both the transverse (y) and longitudinal (x) strains at one point. Tensile strains occurred in those SGs because the wheel (load) passes in a longitudinal direction far from the instrument, thus causing elongation at some point where slab curvature has shifted in comparison to the curvature under the wheel.

Fig. 12 presents the compressive and tensile stresses for the DWA versus the truck's average speed and the distance of the SWA from the slab edge. The graphs show that the DLTs resulted in coherent measurements for most instruments, although some SGs did not work, as is reasonable for such a practical experiment. As for the distance between the truck and the instruments, it would be likely that the bigger the distance the smaller the stresses; this is easily perceivable in DLT01 which passed at a distance of 93 cm, 40% higher than the average distance, thus creating the minimum stresses for all SGs. Regarding the truck's average speed, no variance was noticed when increasing the speed from 10 km/h to around 40 km/h; this observation open contradict other studies that found low-speed or semi-static loads to be more damaging for the pavement [26-28].

The Braking Effect

DLTs 19 and 20 were conducted with a 10 km/h speed and braking with the DWA at the position of SGs 07 and 08, therefor, the only SGs capable of capturing the DWA strains were those before SG07. Fig. 13 presents a stress assessment of the average stresses

Table 3. DLT Stresses (MPa).

	SWA Distance from the Edge (cm)	Avg. Speed (km/h)	SG01		SG03		SG07		SG08		SG09		SG10		SG11		SG16	
			SWA	DWA	SWA	DWA	SWA	DWA	SWA	DWA	SWA	DWA	SWA	DWA	SWA	DWA	SWA	DWA
DLT01	93	6.81	-0.196	-0.607	-0.098	-0.389	NA	0.290	NA	0.223	NA	0.223	NA	0.218	NA	NA	-0.334	-1.257
DLT02	59	6.72	-0.266	-0.854	-0.122	-0.533	0.147	0.326	NA	0.260	0,074	0.296	NA	0.258	NA	NA	-0.482	-1.554
DLT03	54	7.27	-0.193	-0.799	-0.073	-0.537	0.147	0.363	NA	0.333	NA	0.298	NA	NA	NA	0.187	-0.407	-1.806
DLT04	56	7.59	-0.267	-0.848	NA	-0.633	NA	0.254	NA	0.334	NA	0.256	NA	1.865	NA	NA	-0.481	-1.955
DLT05	62	7.28	-0.244	-0.921	-0.148	-0.635	NA	0.290	NA	0.368	NA	0.218	NA	NA	NA	NA	-0.330	-1.804
DLT06	57	6.44	-0.291	-1.042	NA	-0.731	NA	0.254	NA	NA	NA	0.296	NA	NA	NA	NA	-0.405	-1.695
DLT07	59	8.48	-0.266	-0.920	-0.144	-0.610	0.147	0.327	NA	NA	NA	0.260	NA	0.258	NA	NA	-0.295	-1.991
DLT08	58	8.51	-0.242	-0.991	NA	-0.729	NA	0.290	NA	NA	NA	0.184	NA	0.258	NA	0.184	-0.479	-1.809
DLT09	65	8.48	-0.242	-0.871	-0.170	-0.633	NA	0.290	NA	0.368	NA	0.336	NA	0.258	NA	0.256	-0.403	-1.621
DLT10	48	9.08	-0.267	-1.043	-0.097	-0.683	NA	0.326	NA	0.368	NA	0.185	NA	NA	NA	NA	-0.368	-1.770
DLT11	62	9.01	-0.244	-0.899	-0.146	-0.582	NA	0.326	NA	0.407	NA	0.223	NA	0.147	NA	NA	-0.370	-1.844
DLT12	47	8.86	-0.316	-1.066	-0.244	-0.723	NA	0.326	NA	NA	NA	0.293	NA	NA	NA	NA	-0.480	-1.846
DLT13	48	9.08	-0.291	-1.139	-0.171	-0.538	NA	0.349	NA	NA	NA	0.221	NA	NA	NA	NA	-0.481	-1.957
DLT14	58	10.10	-0.217	-0.993	-0.148	-0.636	NA	0.290	NA	0.370	NA	0.298	NA	0.223	NA	NA	-0.407	-1.920
DLT15	57	8.45	-0.267	-0.993	-0.195	-0.659	NA	0.326	NA	0.296	NA	0.293	NA	NA	NA	NA	-0.440	-1.809
DLT16	44	32.40	-0.171	-0.850	-0.122	-0.585	NA	0.218	NA	0.368	NA	0.333	NA	0.293	NA	0.257	-0.185	-1.737
DLT17	39	42.00	-0.267	-1.019	-0.122	-0.560	NA	0.268	NA	0.368	NA	0.295	NA	NA	NA	0.184	-0.405	-1.771
DLT18	37	43.68	-0.195	-1.043	-0.196	-0.753	0.183	0.365	NA	0.405	NA	0.256	NA	NA	NA	0.184	-0.479	-1.984
DLT19	55	12.30	NA	-0.726	NA	-0.232	NA	NA	NA	NA	NA	NA	NA	NA	NA	NA	-0.479	-1.367
DLT20	54	12.60	-0.436	NA	-0.146	-0.146	NA	NA	NA	NA	NA	NA	NA	NA	NA	NA	-0.445	-1.292

NA = not Able to Measure

Table 4. DLT Stresses (MPa): Part II.

	SWA Distance from the Edge (cm)	Avg. Speed (km/h)	SG18		SG22		SG25		SG26		SG29		SG30		SG31	
			SWA	DWA	SWA	DWA	SWA	DWA	SWA	DWA	SWA	DWA	SWA	DWA	SWA	DWA
DLT01	93	6.81	NA	-0.291	NA	-0.216	NA	-0.290	NA	0.188	NA	0.286	NA	-0.437	0.147	0.473
DLT02	59	6.72	-0.121	-0.436	NA	-0.312	NA	NA	NA	0.253	NA	0.433	NA	-0.653	0.109	0.656
DLT03	54	7.27	NA	-0.389	NA	-0.309	NA	-0.328	NA	0.274	0.218	0.508	NA	-0.644	0.145	0.874
DLT04	56	7.59	NA	-0.437	NA	-0.557	NA	-0.546	NA	0.214	NA	0.544	-0.152	-0.764	0.256	0.907
DLT05	62	7.28	NA	-0.460	NA	-0.541	NA	-0.544	NA	NA	NA	0.580	NA	-0.691	NA	0.945
DLT06	57	6.44	NA	-0.532	-0.143	-0,398	NA	-0.615	NA	0.255	NA	0.691	NA	-0.525	NA	0.764
DLT07	59	8.48	-0.144	-0.435	NA	-0.360	NA	NA	NA	0.327	NA	0.580	NA	-0.691	0.218	0.508
DLT08	58	8.51	-0.169	-0.483	NA	-0.406	NA	-0.542	NA	0.217	NA	0.545	NA	-0.731	0.218	2.001
DLT09	65	8.48	NA	-0.386	NA	-0.473	NA	-0.399	NA	0.290	NA	0.508	-0.181	-0.655	0.509	1.493
DLT10	48	9.08	-0.145	-0.606	NA	-0.384	NA	-0.717	NA	0.325	NA	0.546	NA	-0.765	0.545	0.508
DLT11	62	9.01	-0.097	-0.411	-0.144	-0.539	NA	-0.500	NA	0.289	0.181	0.508	-0.183	-0.731	NA	NA
DLT12	47	8.86	-0.120	-0.460	-0.120	-0.288	NA	NA	NA	0.286	0.181	0.616	-0.257	-0.874	NA	1.090
DLT13	48	9.08	-0.122	-0.533	NA	-0.408	NA	-0.506	NA	0.290	0.181	0.613	NA	-0.799	NA	0.763
DLT14	58	10.10	-0.146	-0.460	-0.168	-0.335	NA	-0.504	0.111	0.290	0.147	0.544	-0.254	-0.762	0.216	0.470
DLT15	57	8.45	-0.098	-0.461	NA	NA	NA	-0.468	NA	0.214	0.214	0.544	NA	-0,691	NA	NA
DLT16	44	32.40	-0.097	-0.374	NA	-0.455	NA	-0.398	NA	0.288	NA	0.506	-0.182	-0.690	NA	NA
DLT17	39	42.00	-0.146	-0.487	NA	NA	-0.214	-0.540	0.147	0.396	0.181	0.546	-0.143	-0.728	NA	NA
DLT18	37	43.68	-0.097	-0.411	NA	NA	NA	-0.508	NA	0.250	0.183	0.617	-0.183	-0.762	NA	NA
DLT19	55	12.30	NA	-0.362	NA	NA	NA	NA	NA	0.218	NA	0.254	-0.219	-0.513	0.254	NA
DLT20	54	12.60	-0.145	NA	-0.119	NA	NA	NA	NA	0.218	NA	NA	-0.107	-0.437	0363	0.689

NA = Not Able to Measure

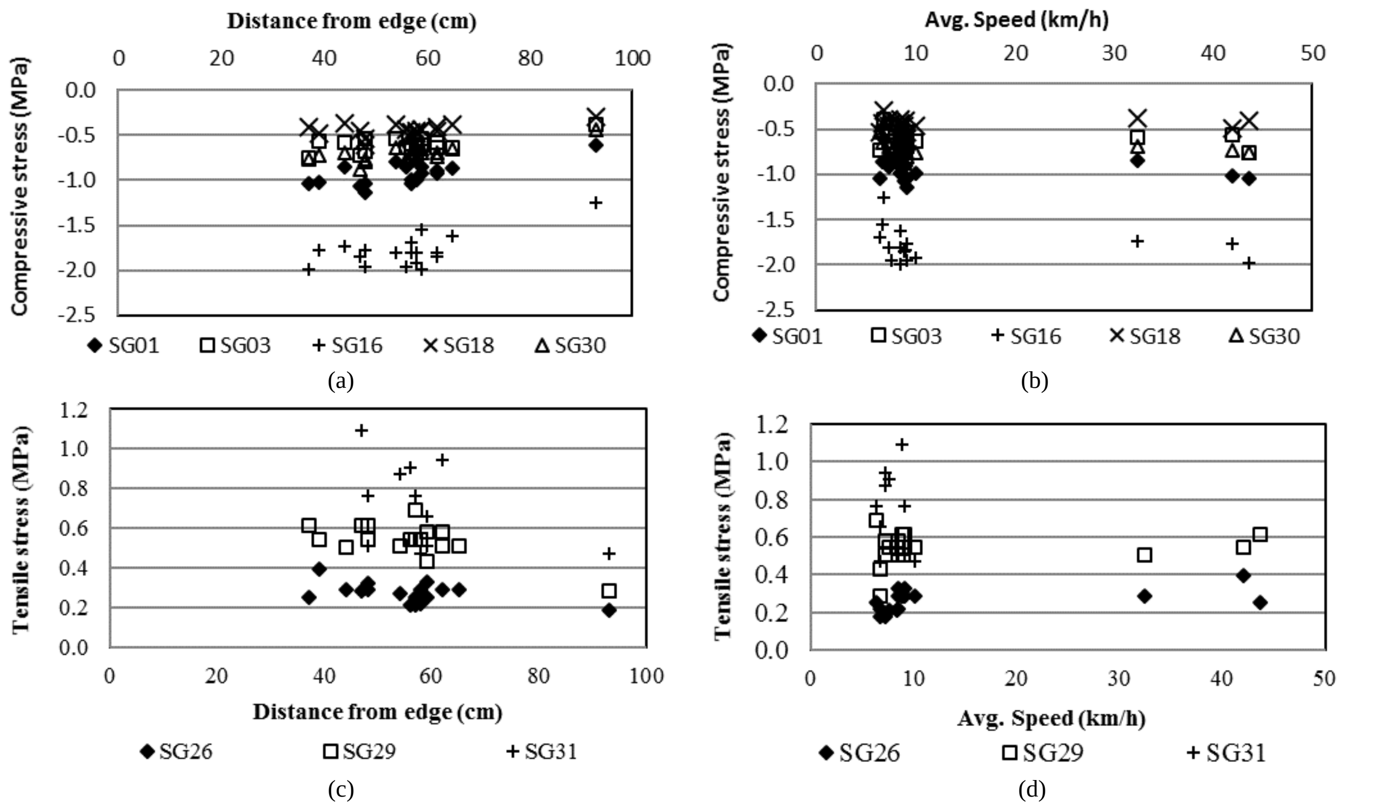

Fig. 12. Compressive Stresses Versus Distance from Edge (a) and Average Speed (b); Tensile Stresses Versus Distance from Edge (c) and Average Speed (d).

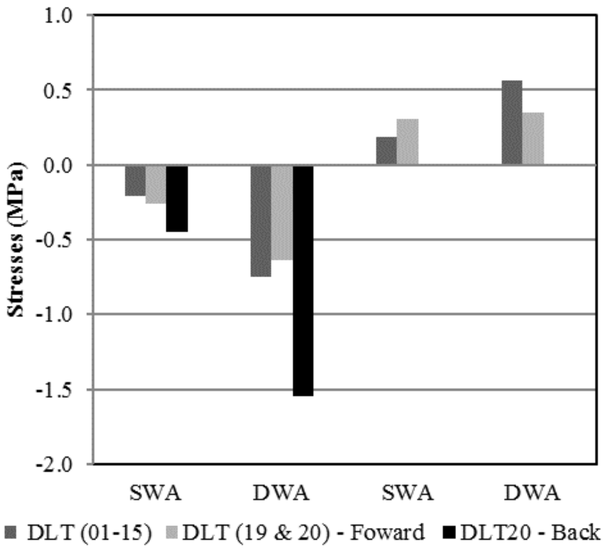

Fig. 13. Stresses from Different Operations.

measured by 10 km/h constant speed DLTs (01 to 15), braking DLTs in "forward" operation (19 and 20) and braking DLT in "back" operation (20). Unfortunately, the "back" operation in DLT19 was not visible in the strain graphs. The SWA stresses were increased in 19% (compressive) and 40% (tensile) when the truck was braking. Conversely, the DWA stresses were 18% (compressive) and 63% (tensile) higher when the truck was at constant speed without braking. This happens due to the front wheel braking inducing a displacement of the vehicle's mass center, which causes a load increase on the front wheels. This idea would also explain the fact that DWA stresses were lower in braking DLTs when compared to constant speed DLTs. In the first case, the DWA would be momentarily less loaded. Concerning the "back" compressive stresses in DLT20, the values were quite greater than those of constant speed DLTs. This difference can be explained by the fact that the operation in return gear was done with a less than 4 km/h speed. Hence, for this case, keeping with the studies previously mentioned, the slower truck speed is associated with higher strains in the pavement. Supposedly, only less than 10 km/h, *i.e.,* low speeds, are more harmful to the structure and that speeds above 10 km/h are equal in effect.

Analysis of Slab Stress State

With the tensile and compressive stresses and accurate knowledge of the SG's position it was possible to draw the slab stresses diagram. Due to a "concrete foot" found in the last few slab inches, SG 26 and 31 are fixed, respectively, 90 and 70 mm from the slab bottom. Therefore, the stresses calculated are not properly the bottom ones; likewise the top stresses are in reality those associated with instruments that are positioned 10 mm from the surface. By extending the diagram stress line it was possible to estimate the maximum bottom and top stresses; in addition, the neutral axis position was determined, as measured from the slab bottom. These data are shown in Table 5.

It is clear the bottom stresses upgrade when accounting for the actual slab bottom and not the SG position. Several instruments indicated stresses above 1.0 MPa with a maximum value of 3.2 MPa. Although below the concrete design strength (4.5 MPa) these are not insignificant. The slab high stiffness (42,000 MPa) on SG31 and 30 positions can explain these stress values. For the top instruments, the extrapolation in only 10 mm did not change significantly the stresses. Surface instruments, like SG16, still measure greater stresses because of its transversal proximity to the load. The average neutral axis position was at 155 mm above the slab's bottom. In an ideal situation it is expected that the neutral axis would be placed exactly at the slab half thickness; yet, external factor such as poor concrete densification, mixing and curing can dislocate the neutral axis. For the short CRCP, the displacement found for the neutral axis was 35 mm above the slab half thickness; despite the

Table 5. Top-Bottom Analysis.

	SG 30 -31						SG 25 – 26			
	SWA			DWA			DWA			
DLT	TOP (MPa)	BOTTOM (MPa)	Neutral Axis (mm)	TOP (MPa)	BOTTOM (MPa)	Neutral Axis (mm)	DLT	TOP (MPa)	BOTTOM (MPa)	Neutral Axis (mm)
DLT01	NA	NA	NA	-0.494	0.871	153.2	DLT01	-0.324	0.495	145.1
DLT02	NA	NA	NA	-0.735	1.229	150.2	DLT03	-0.371	0.661	153.7
DLT03	NA	NA	NA	-0.739	1.538	162.1	DLT04	-0.600	0.703	129.4
DLT04	-0.170	0.435	170.4	-0.868	1.638	156.8	DLT06	-0.677	0.814	131.0
DLT05	NA	NA	NA	-0.793	1.661	162.4	DLT08	-0.596	0.705	130.0
DLT06	NA	NA	NA	-0.525	1.328	164.8	DLT09	-0.448	0.733	148.9
DLT07	NA	NA	NA	-0.766	1.033	137.8	DLT10	-0.791	0.995	133.7
DLT08	NA	NA	NA	-0.902	3.196	187.2	DLT11	-0.556	0.796	141.3
DLT09	-0.224	0.811	188.0	-0.789	2.433	181.2	DLT13	-0.563	0.802	141.0
DLT10	NA	NA	NA	-0.845	1.065	133.8	DLT14	-0.561	0.800	141.1
DLT12	NA	NA	NA	-0.997	1.949	158.8	DLT15	-0.517	0.652	133.9
DLT13	NA	NA	NA	-0.897	1.446	148.2	DLT16	-0.447	0.729	148.8
DLT14	-0.285	0.422	143.5	-0.839	1.006	130.9	DLT17	-0.607	0.998	149.2
DLT19	-0.249	0.460	155.8	NA	NA	NA	DLT18	-0.562	0.737	136.2
DLT20	-0.136	0.569	193.6	-0.507	1.182	167.9				

constructive problems aforementioned, it is only intuitive to think that the longitudinal steel (placed 20 mm above the slab half-height) that is pulling up the neutral axis.

Conclusions

Four experimental continuously reinforced concrete pavement (CRCP) sections with different percentages of longitudinal steel were built in São Paulo, Brazil. The short CRCP cracks exhibited crack patterns that are very different from conventional CRCP cracking patterns. Of all those dissimilarities the most noticeable is the time required for cracking to appear at the concrete surface; it took over one year for the first crack to show up at the slab surface of Section 3 and Section 1, of submittal of this paper, has no cracking at all. Consequently, the resulting crack spacing in the four experimental short-length sections was larger than any traditional CRCP mentioned in the literature. Nevertheless, the crack width at the experimental sections surface was similar to that of traditional CRCP. The crack spacing patterns verified in the sections (3 and 4) allows to conclude that, for design purposes, critical stresses on concrete slabs are to be similar to dowelled jointed plain concrete, because the slabs geometry are close to plain concrete slabs.

The FWD testing of the short CRCP sections disclosed great interlock action at the crack according the measured LTE (higher than 90% for all cracks). Deflections measured between cracks and at the cracks were very similar pointing out a continuous structural behaviour even in a physical discontinuity.

The backcalculation showed values of E and k much lower in the slab edge pointing out that the higher deflections may be causing some concrete deterioration at those points. However, for Section 2 with the higher steel amount, the backcalculated modulus (even at the edge) were greater due to longitudinal steel increasing slab stiffness.

Regarding dynamic load tests with a truck, the main findings were: (1) increasing the vehicle speed from 10 to 40 km/h did not affect the stresses; (2) braking shifts the load effects of frontal and rear axles; (3) the higher tensile stress measured at the slab bottom was 3.2 MPa yet below the concrete design flexural strength of 4.5 MPa; and (4) the neutral axis was verified to be above the slab half-height, thus proving the increasing effect of the longitudinal steel area has in the slab stiffness.

Despite its diverse crack spacing when compared to traditional CRCP, the short-length CRCP seems to be performing rather well when compared to asphalt and JPC pavements constructed at the same time in bus corridors and bus terminals in São Paulo. The cracks are tight and uniform resulting in adequate load transfer. However, an anchorage system at the slab end should be provided for the design of future short-sections, as lack of anchorage proved to be harmful to the concrete edges while also making the crack spacing larger.

Acknowledgements

The authors are very grateful to the State of São Paulo Research Foundation (FAPESP) for their support to the research developed at the University of São Paulo aiming to develop designs and construction techniques for concrete pavements in the country, through process #98/11629-5 and CAPES - Ministry of Education – for the scholarship provided to the first author.

References

1. Balbo, J.T. (2009). *Concrete Pavements* (in Portuguese). Oficina de Textos, São Paulo, Brazil.
2. Liu, C, Wang, Z., and Lee, J.N. (2008). Influence of concrete joints on roughness index and pavement serviceability. *International Journal of Pavement Research and Technology*, 1(4), pp. 143-147.
3. Kohler, E. and Roesler, J. (2004). Active crack control for continuously reinforced concrete pavements. *Transportation Research Record*, No. 1900, pp. 19 – 29.
4. Dossey, T. and Hudson, W.R. (1994). Distress as function of age in continuously reinforced concrete pavements: models developed for Texas pavement management information system. *Transportation Research Record*, No. 1455, pp. 159 – 165.
5. Tayabji, S.D., Stephanos, P.J. and Zollinger, D.G. (1995). Nationwide field investigation of continuously reinforced concrete pavements. *Transportation Research Record*, No. 1482, pp. 7 – 18.
6. Gharaibeh, N.G., Darter, M.I., and Heckel, L.B. (1999). Field performance of continuously reinforced concrete pavement in Illinois. *Transportation Research Record*, No. 1684, pp. 44 – 50.
7. Won, M.C. (2011). Continuously reinforced concrete pavement: identification of distress mechanisms and improvement of mechanistic-empirical design procedures. *Transportation Research Record*, No. 2226, pp. 51 – 59.
8. Schindler, A.K. and McCullough, B.F. (2002). Importance of concrete temperature control during concrete pavement construction in hot weather conditions. *Transportation Research Record*, No. 1813, pp. 3 – 10.
9. McCullough, B.F. and Dossey, T. (1999). Considerations for high-performance concrete paving. Recommendations from 20 years field experience in Texas. *Transportation Research Record*, No. 1684, pp. 17 – 24.
10. Johnston, D.P. and Surdahl, R.W. (2006). Effects of base type modelling long-term pavement performance of continuously reinforced concrete sections. *Transportation Research Record*, No. 1979, pp. 93 – 101.
11. Balbo, J.T., Massola, A., and Pereira, D. (2012). Structural aspects of the experimental CRCP in São Paulo. *Proceedings of the 10th International Conference on Concrete Pavements*, International Society for Concrete Pavements, Quebec, Canada.
12. Zhang, H.L. and Wang, Y.H. (2011). Measurement and analysis of early-age strain and stress in continuously reinforced concrete pavement. *International Journal of Pavement Research and Technology*, 4(2), pp. 89-96.
13. Tayabji, S.D., Stephanos, P.J., Gagnon, J.S. and Zollinger, D.G. (1998). Performance of Continuously Reinforced Concrete Pavement. Volume II: Field Investigations of CRC Pavements. *FHWA-RD-94-149*, FHWA, U.S. Department of Transportation, Washington, DC, USA.
14. Tayabji, S.D., Zollinger, D.G., Veredey, J.R., and Gagnon, J.S. (1998). Performance of Continuously Reinforced Concrete

Pavements. Volume III: Analysis and Evaluation of Field Test Data. *FHWA-RD-94-180*, FHWA, U.S. Department of Transportation, Washington, DC, USA.
15. Nam, J.H., Kim, S.M., and Won, M.C. (2007). Variation of crack width over time in continuously reinforced concrete pavement. *Transportation Research Record*, No. 2037, pp. 3 – 11.
16. Liu, J., Zollinger, D.G., and Li, P. (2008). Feasibility of using accelerated thin bonded concrete overlay for CRCP spalling repair. *International Journal of Pavement Research and Technology*, 1(3), pp. 113-120.
17. American Association of State Highway and Transportation Officials (1993). Guide for design of pavement structures. AASHTO, Washington, DC, USA.
18. Davids, W. (2004). EverFE: Software for the 3D Finite Element Analysis of Jointed Plain Concrete Pavements. (Available at: http://www.civil.umaine.edu/everfe/).
19. Shahin, M.Y. (1985). Use of the falling weight deflectometer for the non-destructive deflection testing of jointed concrete airfield pavements. *Proceedings of the 3rd International Conference on Concrete Pavement Design and Rehabilitation*, Purdue University, pp. 549-556.
20. Vandebossche, J.M. (2007). Effects of slab temperature profiles on the use of falling weight deflectometer data to monitor joint performance and detect voids. *Proceedings of the Transportation Research Board Annual Meeting*, Washington, DC, USA.
21. Colim, G.M., Balbo J.T., and Khazanovich, L. (2011). Effects of temperature changes on load transfer in plain concrete pavement joints. *Ibracon Structures and Materials Journal*, 4(3), pp. 407-439.
22. Zollinger, D.G. and Barenberg, E.J. (1990). Mechanistic design considerations for punchout distress in continuously reinforced concrete pavement. *Transportation Research Record*, No. 1286, pp. 25 – 37.
23. Jeong, J.H. and Zollinger, D.G. (2001). Characterization of stiffness parameters in design of continuously reinforced and jointed pavements. *Transportation Research Record*, No. 1778, pp. 54 – 63.
24. Hall, K.T. (1991). Performance, evaluation and rehabilitation of asphalt-overlaid concrete pavements. *Ph.D. Dissertation*. University of Illinois, Urbana-Champaign, Illinois, USA.
25. Crovetti, J.A. (1997). Design and evaluation of jointed concrete pavement systems incorporating open-graded permeable bases. *Ph.D. Dissertation*, University of Illinois, Urbana-Champaign, Illinois, USA.
26. Kim, S.M., Won, M.C., and McCullough, B.F. (2002). Dynamic stresses response of concrete pavements to moving tandem-axle loads. *Transportation Research Record*, No. 1809, pp. 32-41.
27. Zhang, W., Wang, G., Ma, S., and Li, X. (2007). Field experimental study on measurement and analysis strain on the rigid pavement slab subjected to moving vehicle loads. *Proceedings of the International Conference on Transportation Engineering (ICTE)*, China.
28. Xiao, T., Sun, J.S., Wang, X.H., and Chen, Z.X. (2011). Dynamic response analysis of cement concrete pavement under different vehicle speeds. *Geotechnical Special Publication*, No. 212, ASCE, Washington, DC, USA.